Available online at www.sciencedirect.com
SCIENCE DIRECT®
Journal of Sound and Vibration 277 (2004) 101–122
JOURNAL OF SOUND AND VIBRATION
www.elsevier.com/locate/jsvi

Creating high level sound in a duct using an axial array of sources

M.E. Johnson, C.R. Fuller*

Virginia Tech, Vibration and Acoustics Laboratories, Durham Hall, MC 0238, Blacksburg, VA 24060, USA

Received 5 October 2001; accepted 22 August 2003

Abstract

In this paper, both a frequency domain method for creating high level harmonic excitation and a time domain inverse method for creating large pulses in a duct are developed. To create controllable, high level sound an axial array of six JBL-2485 compression drivers was used. The pressure downstream is considered as input voltages to the sources filtered by the natural dynamics of the sources and the duct. It is shown that this dynamic behavior can be compensated for by filtering the inputs such that both time delays and phase changes are taken into account. The methods developed maximize the sound output while (1) keeping within the voltage constraints of the sources and (2) maintaining a suitable level of reproduction accuracy. For harmonic excitation, pressure levels of over 155 dB were created experimentally over a wide frequency range (1000–4000 Hz). For pulse excitation there is a tradeoff between accuracy of reproduction and sound level achieved. However, the accurate reproduction of a pulse with a maximum pressure level over 6500 Pa was achieved experimentally. It was also shown that the compliance of the throat connecting the driver to the duct makes it difficult to inject sound into any of the cut-on modes in the duct just below the cut-on frequency of each new acoustic mode (pre cut-on loading effect).

1. Introduction

For the purposes of developing time domain models of the acoustic properties of liner facesheets in realistic application conditions it was desired that high acoustic levels be created in a $0.05\,\mathrm{m} \times 0.05\,\mathrm{m}$ cross-section duct. In general, the purpose of the duct is to assess the acoustic characteristics of acoustic liner components in the presence of acoustic signals that are representative of those found near the fan in commercial aircraft engines. Specifically, the

*Corresponding author. Department of Mechanical Engineering, Virginia Polytechnic Institute and State University, 133 Durham Hall, Mail code 2038, Blacksburg, VA 24061-0238, USA. Tel.: +1-540-231-4162; fax: +1-540-231-8836.
E-mail address: martyj@vt.edu, c.r.fuller@larc.nasa.gov (C.R. Fuller).

0022-460X/$ - see front matter
doi:10.1016/j.jsv.2003.08.031

requirements were that: (1) the sound pressure levels be in the order of 160 dB, (2) the waves created were travelling waves (i.e., not standing waves) and (3) the frequency of harmonic signals (500–6000 Hz) and the shapes of pulses were easily altered depending on the desired test case. Preliminary work at the Flow Impedance Test Facility at NASA Langley had shown that it was difficult to produce sound levels greater than 150 dB above 1 kHz when a number of JBL-2485 compression drivers were connected to the duct at a single junction.

This paper describes a method of achieving the requirements stated above using an axial array of sources mounted on a duct. This work can be neatly divided into two parts: (1) investigation into source–duct interaction and the implications for source design and placement and (2) development of methods for maximizing the outputs from a set of given sources. The theory developed in the first section of the paper is then validated experimentally and it is shown that broadly speaking the requirements outlined above can be met.

Two test rigs were developed, the first of which was an 2.4 m long closed duct with anechoic terminations used as a preliminary test bed for testing sources and optimization routines and the second of which was a long open ended duct with sources mounted at one end and an anechoic muffler section fitted to the other end used for the full scale demonstration of the technology. Fig. 1 shows a schematic of both ducts with sources mounted on the sides. In both ducts flush mounted microphones were used to monitor the sound levels downstream from the sources. For the configurations shown in Fig. 1 the sources radiate sound in both directions in the duct. The sound travelling upstream can then be reflected off of the open end of the duct (for the second duct) and also off of the other sources connected to the duct. All of these reflections add dynamic behavior to the system that in effect "filters" the signals as they go from the input to the sources to the downstream microphones. Previously, adaptive filters have been used to compensate for system dynamics [1,2] but this work will rely on an inverse filtering method which maximizes the sound power output.

To investigate the interaction of a source with the duct an analytical model of a source mounted to the duct was developed and the properties of the source were altered to show their effect on performance. Since higher order modes cut-on within the frequency span of interest the duct was

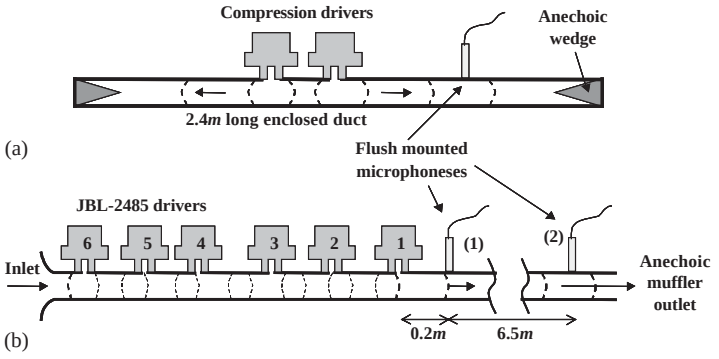

Fig. 1. A schematic of the two ducts used to test the techniques developed in this paper. (a) Duct #1 is a 2.4 m long anechoically terminated duct used as a test bed and duct. (b) Duct #2 is a long open ended duct with an anechoic muffler outlet at one end. A six source array was used for the tests on this duct. In both ducts flush mounted microphones were used to monitor the downstream sound pressure levels.

modelled using a modal summation of propagating and non-propagating acoustic modes. The results were then validated experimentally and the results presented.

To maximize the signal at a downstream microphone it is necessary to compensate for the source–duct dynamics. To do this each of the sources needs to be driven with a different signal such that the waves created by the sources downstream from the source section all re-enforced each other. To calculate the optimal drive signals to produce high level harmonic waves, a frequency domain phase compensation method was developed. To calculate the optimal drive signals for creating pulses a time domain inverse method was employed. Both of these methods are based on the measurement of the transfer functions between the inputs to the sources and the output of a flush mounted microphone placed downstream in the duct. These techniques were also tested experimentally and results presented.

2. Theory

2.1. Duct acoustics and source–duct interaction

2.1.1. Source–duct interaction

To investigate the interaction of a source driving into a duct a simple theoretical model was constructed using an impedance approach (for further reading on impedance methods see, Ref. [3]). For this work compression drivers were used as sources and a schematic of such a driver is shown in Fig. 2. These drivers are electro-mechanical devices that use an electrical coil to create a force on a stiff diaphragm proportional to the input current. Compression drivers are typically used to drive mid to high frequency horns for sound re-enforcement systems and were chosen for

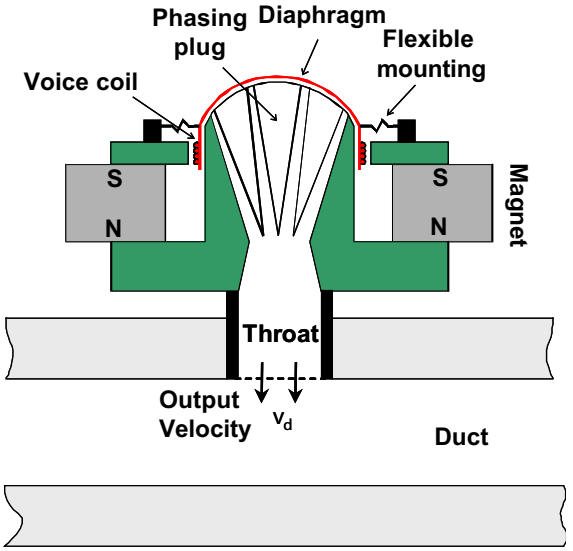

Fig. 2. A schematic of a typical compression driver. An alternating current in the voice coil drives the diaphragm that in turn excites the fluid through a phasing plug and throat.

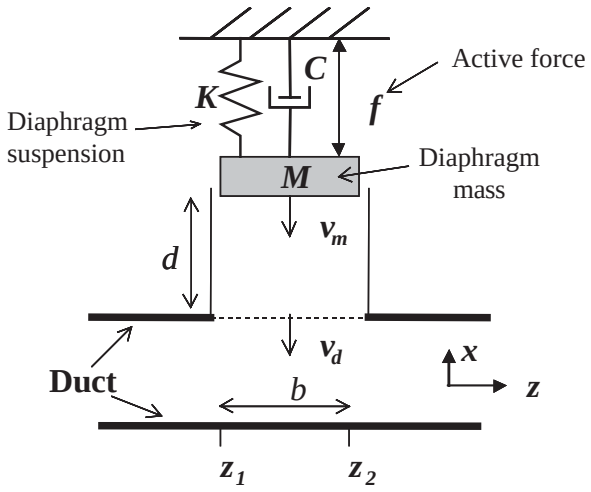

Fig. 3. Schematic of an actuator mounted onto the side of a duct. The actuator is of length b and is positioned between z_1 and z_2. The diaphragm is coupled to the duct through a throat of length d.

this work because of the high frequency range of interest and the potentially high impedance loads. For this work the source is modelled as a mass–spring–damper system driven by a force f (Fig. 3). For an electromagnetic driver this force is proportional to the current applied to the voice coil. The velocity v_m of the diaphragm (mass) drives a short throat modelled as a duct of finite length d. The particle velocity at the throat–duct interface v_d is assumed to be uniform across the throat (i.e., no cross modes in the throat).

If the actuator is driven and is the only source operating then the force (pressure times cross-sectional area) at the throat–duct interface f_d is determined by the input impedance into the duct Z_d:

$$f_d = Z_d v_d = Z_{T2} v_m - Z_{T1} v_d. \tag{1}$$

Since the force f_d (or pressure) on either side of the interface is equivalent it can also be written in terms of input impedance Z_{T1} and the transfer impedance Z_{T2} of the throat. Re-arranging Eq. (1) allows the velocity at the interface to be expressed as a function of the velocity of the mass and the impedances as

$$v_d = \frac{Z_{T2}}{Z_d + Z_{T1}} v_m. \tag{2}$$

If the impedance of the duct is much higher than the impedance in the throat then there will be little motion at the throat–duct interface. However, if the throat is very short, then the throat impedances Z_{T1} and Z_{T2} are equal and large and the velocity at the throat–duct interface matches the velocity of the diaphragm mass.

The motion of the mass will be determined by the input force f, the internal impedance of the source Z_m and the velocity at the throat–duct interface

$$f = [Z_m + Z_{T1}] v_m - Z_{T2} v_d. \tag{3}$$

By combining Eqs. (2) and (3), the velocity at the throat–duct interface can be written as a function of the input force as

$$v_d = \left[[Z_m + Z_{T1}] \left[\frac{Z_d + Z_{T1}}{Z_{T2}} \right] - Z_{T2} \right]^{-1} f. \tag{4}$$

The equations for Z_m, Z_d, Z_{T1} and Z_{T2} are presented in the following sections. If these impedances are known then the velocity at the throat–duct interface can be calculated and from this the sound pressure at a point (x, y, z) downstream in the duct can be calculated as

$$p(x, y, z) = T(x, y, z) v_d, \tag{5}$$

where the function T relates the pressure at any point downstream in the duct due to the motion of a piston on the duct wall (piston same dimensions as one used to calculate Z_d, Z_{T1} and Z_{T2}).

2.1.2. Source internal impedance

The internal impedance of the source is given by [4]

$$Z_m = \mathrm{j}\omega M + C + K/(\mathrm{j}\omega), \tag{6}$$

where j is the imaginary number, ω is the angular frequency, M is the diaphragm mass, C is the damping coefficient and K is the suspension stiffness.

2.1.3. Throat impedance

The assumption made is that the velocity and pressure across the throat is uniform. This is not an unreasonable assumption as long as the diaphragm motion is uniform. The throat can, therefore, be modelled as a closed tube of length d (Fig. 3) driven by a piston at either end. The self and transfer impedances are given by [5]

$$Z_{T1} = \frac{-\mathrm{j}\rho c S_T \cos(kd)}{\sin(kd)}, \quad Z_{T2} = \frac{-\mathrm{j}\rho c S_T}{\sin(kd)}, \tag{7}$$

where the density of the fluid is given by ρ ($1.19\,\mathrm{kg\,m^{-3}}$ for air), c is the speed of sound ($343\,\mathrm{m\,s^{-1}}$ for air), S_T is the cross-sectional area of the throat and k is the acoustic wavenumber given by $k = \omega/c$. To add some damping to the throat (and duct when necessary) a complex wavenumber [6] was used by substituting $k' = k(1 - \mathrm{j}\alpha)$ where α is a small damping term ($\alpha \ll 1$). This is similar to using a complex stiffness in the analysis of vibration [7].

2.1.4. Duct impedance

The duct impedance Z_d is determined by modelling the sound in an infinite duct (of cross-section l_x, l_y) as a series of propagating and non-propagating modes. The derivation follows the work of Smith and Burdisso [8] with the simplification that by assuming that the throat acts as a piston spanning the entire duct, only modes across one dimension of the duct need to be considered.

The source is assumed here to be connected to the side of the duct ($x = 0$) and to act as a rigid rectangular piston of length b and of width l_y (i.e., spanning the entire duct). Therefore, only

$m = 0$ modes will be excited by the source (where m is the mode order in the y direction) and therefore the index m will be suppressed for simplicity in the following equations:

The mode shape of the nth mode (assuming $m = 0$) in a rectangular duct is given by [8,9]

$$\psi_n(x) = \Lambda_n \cos(k_n x), \tag{8}$$

where k_n is the wavenumber of the nth order mode (x direction) and Λ_n is a normalization factor for the modes which is given by $\Lambda_n = \sqrt{\varepsilon_n}$ where $\varepsilon_0 = 1$ and $\varepsilon_i = 2$ when $i > 0$. For example, the modes in a duct of dimensions l_x will have wavenumbers in the x direction given by $k_n = n\pi/l_x$. The fluid wavenumber squared must equal the sum of the squared wavenumbers in all orthogonal directions and therefore,

$$k_{z,n} = \sqrt{k^2 - k_n^2} = \sqrt{\left(\frac{\omega}{c}\right)^2 - k_n^2}. \tag{9}$$

If the frequency ω is sufficiently low then the term under the square root becomes negative and the wavenumber in the z direction is imaginary. An imaginary wavenumber corresponds to an exponentially decaying wave that does not propagate energy down the duct. Due to this, each mode has a cut-on frequency above which it propagates and below which it does not. The first (plane wave) mode, which corresponds to $n = 0$, has a cut-on frequency of 0 Hz and therefore propagates at all frequencies. In a $0.05 \times 0.05\,\mathrm{m}^2$, rigid duct filled with air at 20°C (similar to the one tested experimentally) and the first higher order mode ($n = 1$) cuts on at around 3430 Hz.

Using a summation of modes and integrating their effect over the surface of the throat (i.e., piston), the mechanical duct input impedance Z_d seen by a piston can be expressed as [8]

$$Z_d = \sum_{n=0}^{\infty} \frac{\omega \rho \Lambda_n^2 l_y^2}{jSk_{z,n}^2}\left[b - \frac{1}{jk_{z,n}}\left(1 - \mathrm{e}^{-jk_{z,n}b}\right)\right], \tag{10}$$

where S is the cross-sectional area of the duct (i.e., $S = l_x l_y$). This impedance will be very large for small values of $k_{z,n}$ and this occurs near to the cut-on of each mode (see Eq. (9)).

2.1.5. Calculating the downstream pressure due to a piston

The function T (Eq. (5)) that relates the downstream pressure (i.e., $z > z_2$) to the velocity of a piston source on the duct wall can be calculated by integrating over the surface of the piston [8] (again because m is assumed to equal 0, no variation in y exists).

$$T(x,z) = \sum_{n=0}^{\infty} -\frac{\omega \rho \Lambda_n l_y}{2\mathrm{j}Sk_{z,n}^2}\psi_n(x)[1 - \mathrm{e}^{-\mathrm{j}k_{z,n}b}]\,\mathrm{e}^{-\mathrm{j}k_{z,n}(z-z_2)}. \tag{11}$$

This function, like the duct input impedance (Eq. (10)); will be large just above the cut-on of a mode. However, below the cut-on frequency of a mode the last term in Eq. (11) , $\mathrm{e}^{-\mathrm{j}k_{z,n}(z-z_2)}$, is small because $k_{z,n}$ is negative and imaginary (see Eq. (9)) and therefore for any significant distance downstream the pressure due to that mode is small for a given piston velocity (i.e., $\mathrm{e}^{-\mathrm{j}k_{z,n}(z-z_2)} = \mathrm{e}^{-|k_{z,n}|(z-z_2)}$).

2.1.6. Theoretical results and implications

Fig. 4 shows a plot of the equivalent mechanical impedance Z_d seen by a $0.05\,\mathrm{m} \times 0.025\,\mathrm{m}$ (length b) rectangular piston driving into a $0.05\,\mathrm{m} \times 0.05\,\mathrm{m}$ duct calculated using Eq. (10) by

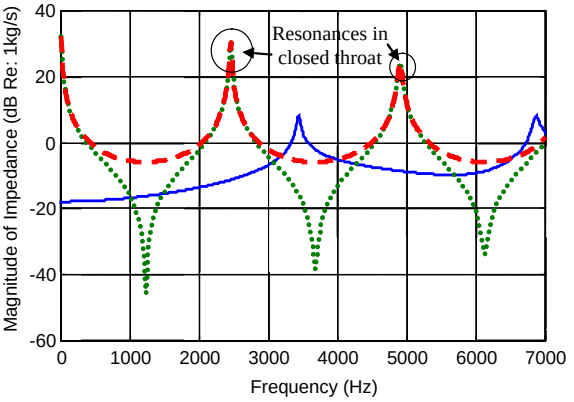

Fig. 4. The equivalent mechanical impedance Z_d (—) seen by a rectangular 0.05 m × 0.025 m piston on the side of a 0.05 m × 0.05 m duct and the input Z_{T1} (···) and Z_{T2} (- - -) cross impedance to a 0.07 m long throat of similar cross-section.

considering the first ten (n) modes. Also shown in Fig. 4 is the input (Z_{T1}) and cross (Z_{T2}) impedance of a 0.07 m long throat, with the same cross-section as the piston, calculated using Eq. (7). The acoustic modes in the throat cause large changes in the impedance over the frequency range of interest. As discussed above, near the cut-on of each mode (i.e., 3430 Hz for the first mode in this example) the duct impedance becomes large and in this example is significantly larger than the throat impedances. This substantially restricts the particle motion at the throat–duct interface (see Eqs. (2) and (4)). In this case the diaphragm simply compresses the air inside the throat. The plots shown in Fig. 4 assume a complex wavenumber in both the duct and throat given as $k' = k(1 - 0.005\mathrm{j})$.

If the throat is very short (i.e., throat impedances are high) then the velocity at the throat–duct interface becomes the same as the velocity of the diaphragm (see Eq. (2)). It is possible that the duct impedance may be large enough to restrict the motion of the diaphragm itself but this will only happen if the magnitude of the internal source impedance (Z_m) is very small (see Eq. (4)). Fig. 5 shows the velocity at the throat–duct interface due to a unit input force ($f = 1$ N) under two circumstances: (1) a throat length $d = 0$ and (2) a throat length of $d = 0.07$ m. For both of these cases the diaphragm is assumed to have a mass of 10 g, a natural frequency of 1500 Hz (in vacuo) and a damping ratio of $\zeta = 0.05$. Other than the main diaphragm resonance there are two other features of importance shown in Fig. 5: (1) increased velocity at throat–duct resonances and (2) decreased velocity around the cut-on of every mode. Since the duct end of the throat is not rigid the throat–duct resonance frequencies are different from the throat resonance frequencies assuming hard ends (Fig. 4). When there is no throat ($d = 0$) the duct impedance is still substantially smaller than the internal impedance of the source and no appreciable reduction in velocity occurs near cut-on. These results show that the presence of the throat can have large effects on actuator performance. The additional dynamic behavior makes it more difficult to obtain an ideally 'flat' frequency response. In other words, if the desired pulse shape is used as an input to the source the response downstream in the duct will not have the desired pulse shape.

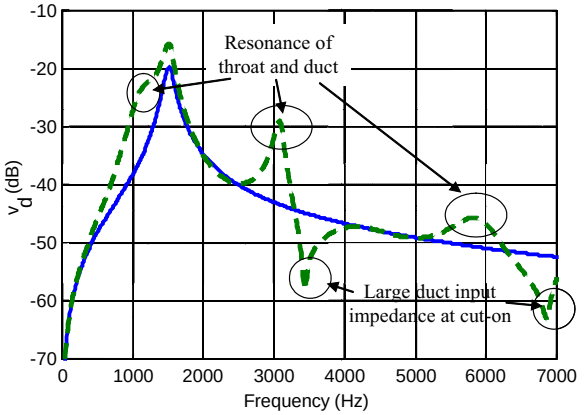

Fig. 5. The velocity at the throat–duct interface due to a unit input force for two different throat lengths $d=0$ (—), $d=0.07$m (- -). The resonance frequency of the source is 1500 Hz.

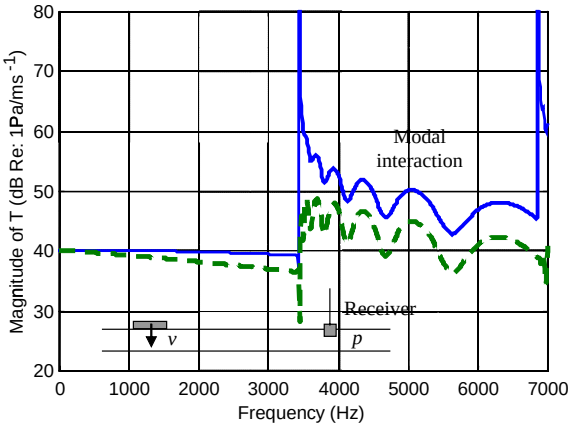

Fig. 6. The acoustic transfer impedance T between the piston source and a position 1 m downstream plotted with damping included ($k' = k(1 - 0.005\text{j})$) (- -) and without losses (—).

Fig. 6 shows the acoustic transfer function T between the piston source and a point on the duct wall 1 m downstream. Two plots are shown, one without damping added and one with damping (i.e., using a complex wavenumber $k' = k(1 - 0.005\text{j})$ in this case). Two effects can be observed here: (1) The transfer function increases as a new mode cuts on (sharply if no losses are included) and (2) above cut-on there is modal interaction which causes numerous dips in the impedance.

By combining the results presented in Figs. 5 and 6 (i.e., T and v_d) the pressure 1 m downstream from a source with a 0.07 m throat driven with a unit input force was calculated and is presented in Fig. 7. Just below cut-on the high impedance due to the $n = 1$ mode reduces the throat–duct velocity and hence reduces the pressure downstream which is transmitted by the $n = 0$ mode alone. Just above cut-on the throat–duct velocity is still restricted but the second mode begins to propagate downstream with relatively high amplitude (Fig. 6).

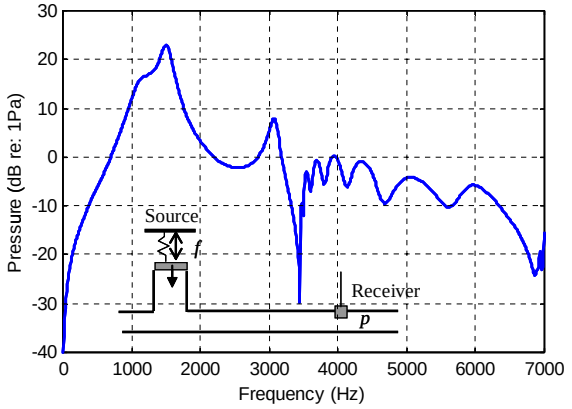

Fig. 7. The pressure 1 m downstream due to a unit input force to the actuator. The source throat has a length of 0.07 m.

These results imply that just below cut-on it may be difficult to inject energy into a duct (pre cut-on loading effect) and above cut-on the interaction of the modes will cause variations in pressure along the duct. Both of these effects will cause the performance of the source to vary with frequency. By using many sources in an axial array the modal interaction problem may be overcome but the pre cut-on impedance loading of the throat will be difficult to overcome unless the throat is removed. It is important to note that the pre cut-on loading effect is caused by modes that are not cut-on restricting the power injected into modes that are already cut-on.

2.1.7. Passive effect of sources

The sources used for this work are "off the shelf" compression drivers that are designed to drive acoustic horns. As shown in Fig. 2, these drivers have significant throat lengths (4 in for the JBL-2485s). Large throat lengths also add significant passive dynamics to waves propagating in the duct such that waves created by one source can have large reflections off of other sources that are lining the duct. Consider for example a plane wave travelling in an infinite duct impinging on a side branch such as the source throat. If only frequencies below the first cut-on are considered then the power reflection coefficient due to the side branch is given by [5]

$$R = \left| \frac{S/(2\rho c)}{Z_{T1}/S_T^2 + S/(2\rho c)} \right|^2, \tag{12}$$

where the impedance of the side branch Z_{T1} is given in Eq. (7). The dynamics of the source diaphragm could be included here but for most examples the effect is minimal. At frequencies where the impedance of the throat is very small, the throat will act as a reflector and these frequencies are given by the anti-resonances of the throat. For a 0.07 m long throat the power reflection coefficient becomes near unity when the throat impedance is small (see Fig. 4), i.e., around 1200, 3700 and 6200 Hz. This implies that if an array of similar sources (i.e., similar throat lengths) are used to drive into a duct then there will be frequencies at which the most upstream sources, for example source 6 in Fig. 1(b), will find it difficult to transfer power downstream to the microphone. The shorter the throat length the less of a problem reflection becomes. If the throat lengths are significant then it is important to space the sources unevenly along the duct so that stop band behavior is reduced.

2.2. Calculating optimal drive signals

The sound pressure measured at a microphone placed downstream in the duct can be represented as the input to the sources filtered by a set of transfer functions. These transfer functions include the source dynamics, the throat dynamics, reflections in the duct off of other sources and the inlet, and any propagation delay down the duct to the microphone. A discrete estimate of this set of transfer functions can be measured by driving the sources sequentially with white noise while monitoring the pressure at the microphone.

2.2.1. A frequency domain method for creating high level tonal noise

The transfer function between the K sources and a single microphone downstream can be represented in the frequency domain so that at any one frequency the resulting pressure $p(\omega)$ can be specified by a vector multiplication of the K complex transfer functions $\mathbf{H}$ and the K complex input signals $\mathbf{v}$:

$$p(\omega) = \mathbf{H}(\omega)\mathbf{v}(\omega) = [H_1(\omega), H_2(\omega), \cdots, H_K(\omega)][v_1(\omega), v_2(\omega), \cdots, v_K(\omega)]^{\mathrm{T}}. \tag{13}$$

If it is assumed that the input signals are of the same amplitude g then the maximum pressure will be created when the pressure downstream due to each of the sources all have the same phase. This can be achieved by driving each source with the negative phase of its corresponding transfer function

$$v_k = g\mathrm{e}^{-\mathrm{j}\alpha_k} \quad \text{where} \quad H_k = |H_k|\mathrm{e}^{\mathrm{j}\alpha_k} \tag{14}$$

and where the phase of the kth transfer function is α_k and g is a real gain (the frequency dependence has been omitted for simplicity). If the input signals specified in Eq. (14) are substituted into Eq. (13) then the pressure will be purely real and given by

$$p(\omega) = g\sum_{k=1}^{K}|H_k|. \tag{15}$$

If the frequency of interest is below the cut-on of the first cross mode in the duct then a single microphone will be sufficient to measure the sound propagation down the duct. However, above cut-on more sensors will be required to determine the behavior of the duct.

Consider a rectangular duct with a large aspect ratio ($l_x \gg l_y$) such that the modes in the x-direction cut-on at much lower frequency than in the y direction (Fig. 8). Take for example the

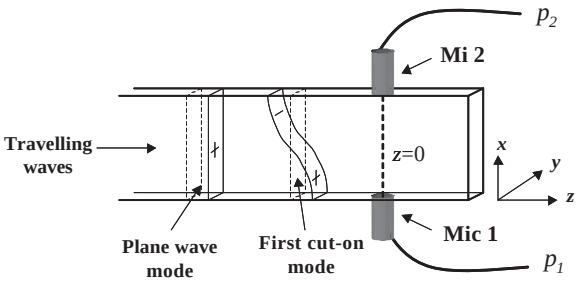

Fig. 8. Using two microphones to detect the plane wave mode and the first cut-on mode in a duct.

case where the frequency range of interest is such that only two modes are cut-on. In this example the pressure **p** measured at two microphones placed on either side of the duct (for simplicity it is assumed that the microphones are at $z = 0$) are due to the amplitudes of the two modes **a** and the values of the mode shapes at the microphone positions (**p** = **Ma**). The measured pressures can, therefore, be used to determine the two mode amplitudes by a simple modal de-convolution ($\mathbf{M}^{-1}$)

$$\mathbf{a} = \mathbf{M}^{-1}\mathbf{p} \quad \Rightarrow \quad \begin{bmatrix} A_0^+ \\ A_1^+ \end{bmatrix} = \begin{bmatrix} 1 & 1 \\ \sqrt{2} & -\sqrt{2} \end{bmatrix}^{-1} \begin{bmatrix} p_1 \\ p_2 \end{bmatrix}. \tag{16}$$

The mode amplitude of the positive travelling plane wave mode ($n = 0$) is A_0^+ and the mode amplitude of the $n = 1$ positive travelling mode is A_1^+. The coefficients in the matrix **M** are determined by the amplitudes of these two modes at the microphone positions (see Eq. (8)).

The output of the two microphones **p** can also be written as a function of the input voltages **v** to the K sources coupled through a transfer function matrix **H**

$$\begin{bmatrix} p_1(\omega) \\ p_2(\omega) \end{bmatrix} = \mathbf{H}(\omega)\mathbf{v}(\omega) = \begin{bmatrix} H_{11}(\omega) & H_{12}(\omega) & \cdots & H_{1K}(\omega) \\ H_{21}(\omega) & H_{22}(\omega) & \cdots & H_{2K}(\omega) \end{bmatrix} \begin{bmatrix} v_1(\omega) \\ v_2(\omega) \\ \vdots \\ v_K(\omega) \end{bmatrix}. \tag{17}$$

Substituting Eq. (17) into Eq. (16) gives $\mathbf{a} = \mathbf{M}^{-1}\mathbf{H}\mathbf{v}$. If $\mathbf{a_d}$ is the normalized vector of desired mode amplitudes and K is larger than two, the system is underdetermined (more inputs than outputs) and there is no unique set of inputs that produces the desired output mode amplitudes. One input $\mathbf{v_0}$ that represents the solution with the smallest summed squared input voltages ($\mathbf{v}^{\mathbf{H}}\mathbf{v}$) can be calculated as [10]

$$v_0 = g(\mathbf{M}^{-1}\mathbf{H})^{\mathrm{H}}\left[\mathbf{M}^{-1}\mathbf{H}(\mathbf{M}^{-1}\mathbf{H})^{\mathbf{H}}\right]^{-1}\mathbf{a_d}. \tag{18}$$

The superscript H denotes a Hermitian or complex conjugate transpose and g is a real gain that can be increased until the voltage limitation of one of the sources is reached.

An alternative way of interpreting this result is to consider the singular value decomposition of the matrix [$\mathbf{M}^{-1}\mathbf{H}$]. The input $\mathbf{v_0}$ calculated using Eq. (18) only excites the first two singular vectors without exciting any of the null-vectors that have no effect on the output.

2.2.2. A time domain method for creating high level pulses

In the time domain the transfer functions between the sources and the downstream microphone can be represented as causal impulse responses and for this work will be represented as an equivalent FIR filter (or equivalently z-transform) with coefficients h_{ki} where the subscript ki denotes the ith filter coefficient between the kth source and the microphone. This representation is sufficiently accurate as long as the sample rate is much higher than the highest frequency of interest and the number of coefficients representing the filter is sufficiently large. This representation is often used for the analysis of active control systems and the reader may refer to Nelson and Elliott et al. [10,11].

The output sampled pressure sequence $p(n)$ is due to the inputs to all K sources and is given by

$$p(n) = \sum_{k=1}^{K} \sum_{i=0}^{I-1} h_{ki} v_k(n-i), \tag{19}$$

where subscript k represents the source number, n is the sample number (or time sequence), I is the number of samples in the FIR impulse response sequence (can be arbitrarily large) and v_k is the input sequence to the kth source. If the input signals are all short sequences of L samples preceded and followed by zeros then the above equation can be rewritten in matrix form

$$\mathbf{p} = \mathbf{H}\mathbf{v}, \tag{20}$$

where the J length output vector $\mathbf{p}$ is given by

$$\mathbf{p} = [p(J-1), p(J-2), \ldots, p(0)]^{\mathrm{T}}. \tag{21}$$

The input vector is made up of K input sequences each of length L. It is assumed that before and after each input sequence the input signals are zero

$$\mathbf{v} = [\mathbf{v}_1, \mathbf{v}_2, \ldots, \mathbf{v}_K]^{\mathrm{T}}, \quad \mathbf{v_k} = [v_k(J-1), v_k(J-2), \ldots, v_k(J-L)]. \tag{22}$$

The matrix $\mathbf{H}$ is made up of K impulse response matrices [12] such that Eq. (20) takes the form

$$[\mathbf{p}] = \begin{bmatrix} [\mathbf{H}_1] & [\mathbf{H}_2] & \cdots & [\mathbf{H}_K] \end{bmatrix} \begin{bmatrix} [\mathbf{v}_1] \\ [\mathbf{v}_2] \\ \vdots \\ [\mathbf{v}_K] \end{bmatrix} \tag{23}$$

and $\mathbf{H_k}$ is a J by L matrix given by

$$\mathbf{H_k} = \begin{bmatrix} h_{k0} & h_{k1} & & \cdots & & h_{k(L-1)} \\ 0 & h_{k0} & h_{k1} & & \ddots & \\ \vdots & 0 & \ddots & & & \\ 0 & \cdots & 0 & h_{k0} & \cdots & h_{k(L-J)} \end{bmatrix}. \tag{24}$$

This matrix formulation assumes that L is larger than J and therefore there is an input v before any output is considered. The objective is to calculate the input sequences that will produce some pre-specified desired output pressure pulse $\mathbf{p_d}$ (normalized). This problem now takes a similar form to that of Eq. (18). The input sequences that produce the desired output while minimizing the sum of the squared input voltages $\mathbf{v}^{\mathbf{H}}\mathbf{v}$ is given by

$$\mathbf{v}_0 = g\mathbf{H}^{\mathrm{T}}\left[\mathbf{H}\mathbf{H}^{\mathrm{T}}\right]^{-1}\mathbf{p_d}, \tag{25}$$

where again g is a real gain that can be increased until the voltage limitation of one of the sources is reached.

The production of virtual acoustic images using arrays of loudspeakers requires the use of similar inverse filtering techniques and the reader may want to refer to the work of Kirkeby and Nelson [13,14].

2.2.3. Effort weighting and error analysis

Depending on the condition of the matrix $\mathbf{HH^T}$ the input can still be very large for a given output. Under these circumstances the efficiency of the system can be improved by including a "conditioning" term and as a result sacrifice accuracy. The conditioning factor β can be added to the diagonal of the $\mathbf{HH^T}$ matrix before inversion

$$\mathbf{v}_e = g\mathbf{H}^{\mathrm{T}}[\mathbf{HH}^{\mathrm{T}} + \beta\mathbf{I}]^{-1}\mathbf{p_d}, \tag{26}$$

where $\mathbf{I}$ is the identity matrix of order J. The term $\beta\mathbf{I}$ effectively increases the eigenvalues of the $[\mathbf{HH^T}]$ matrix by the amount β [15]. With the conditioning term added the output $\mathbf{p}$ does not match the desired output $\mathbf{p_d}$ exactly and a normalize error coefficient E can be defined which describes the accuracy with which the desired signal is reproduced [16]:

$$E = \frac{(\mathbf{p} - \mathbf{p_d})^{\mathbf{T}}(\mathbf{p} - \mathbf{p_d})}{\mathbf{p_d^T p_d}}, \tag{27}$$

where the vector of outputs $\mathbf{p}$ is given by $\mathbf{p} = \mathbf{Hv_e}$. A reasonable compromise must be struck between accuracy and output level. For the experimental results presented further on in this paper an acceptable error level is chosen and the conditioning factor β is increased until this error level is reached.

2.2.4. Maximizing output (loop optimization)

To maximize the pressure in the duct the input gain g (Eqs. (18), (25) and (26)) is increased until the maximum input voltage to the actuators is reached. This maximum input voltage will occur for only *one* of the actuators implying that there is still extra authority left in the other actuators. To make use of this extra authority the source with the largest input voltage is removed from the calculation (Eqs. (18)–(26)) and the calculation repeated with $K - 1$ sources. This new set of input voltages is added to the first set of input voltages and the gain g_1 for this phase of the optimization is increased until one of the $K - 1$ sources reaches the maximum allowable input voltage. This source is now removed from the calculation and the process repeated with $K - 2$ sources and so on until all of the sources have the maximum input gain.

3. Experimental results

The theory presented in previous section was tested on two separate experimental rigs. The first rig was mainly used as a developmental rig (Fig. 1(a)) and was a closed 2.4 m long $0.05\,\mathrm{m} \times 0.05\,\mathrm{m}^2$ cross-sectioned duct made from high density fiberboard. Two 0.3 m long acoustic foam wedges were fitted in either side of this duct producing anechoic conditions above 300 Hz. Both JBL-2485 actuators and Selenium DH200-HM actuators were tested using this rig. The second rig was a 20 m long open ended duct housed at the flow impedance facility at NASA Langley (Fig. 1(b)). Six JBL-2485 sources were mounted onto a square $0.05\,\mathrm{m} \times 0.05\,\mathrm{m}$ steel section of pipe near to the inlet end and coupled to a circular pipe of similar cross section immediately after the source section. About 12 m after the source section the duct was fitted with a long anechoic muffler section before the outlet. The duct was constructed to allow for low speed flow although none of the results presented here were taken under flow conditions. Although there was zero flow

during these tests, the methods described here are based on the measurement of the transfer functions prior to the creation of the actuator drive signals. As long as the transfer functions are measured under the flow conditions of interest and the flow speeds are well below mach = 1 the principle of superposition holds and the methods described here are valid.

To drive the sources a National Instruments eight channel output card (*PCI-6713*) was used. Software was written so that the sources could be driven with independently controlled single frequency or broadband pulses.

3.1. Measurements of duct source interaction

To investigate the source duct interaction and to validate the analytical model developed in the theory section of this paper, a single Selenium DH200-HM actuator was mounted on to the 2.4 m test rig (Duct #1 Fig. 1(a)). The Selenium DH200-HM is a high frequency compression driver (designed to work above 1500 Hz) with a 0.025 m diameter circular throat that is approximately 0.05 m long. The transfer function between the voltage input to the actuator and the output from a microphone placed 1 m downstream was measured and the magnitude is plotted in Fig. 9. This is not identical to the analytical model since the transfer function is between the input voltage and not input current and the output from the microphone. However, the characteristics predicted using the analytical model (Fig. 7) such as the modal interaction and the pre cut-on loading effect appear in this measured response (note: the frequency response values below 1000 Hz are due mainly to noise and should be ignored).

3.2. Multiple sources

The impulse response functions between the six JBL-2485 sources and a single downstream microphone on the open duct (Duct #2, Fig. 1(b)) were measured and the magnitudes are plotted in Fig. 10. There are a number of effects that can be observed. Firstly it can be seen that, like the selenium source, just below cut-on all of the sources are poorly coupled into the duct. This shows that the pre cut-on effect is not source specific and will occur when one or more sources are

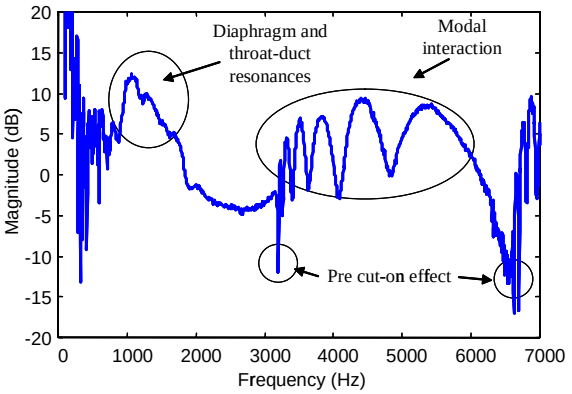

Fig. 9. The measured transfer function between the voltage input to a Selenium DH200-HM and the output of a microphone 1 m downstream. (Note: the *y*-axis is not calibrated and is in dB re: Pa/V units.)

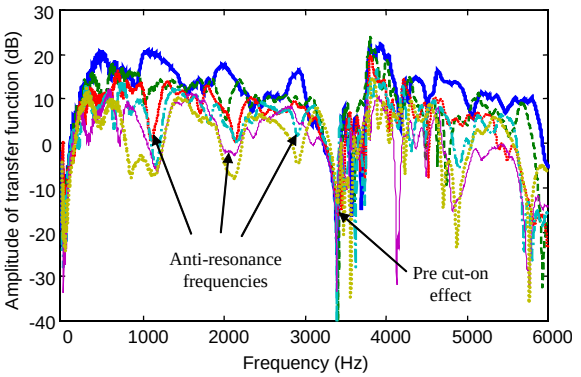

Fig. 10. The measured transfer function between all six JBL-2485 sources and a single downstream microphone. (Note: the y-axis is not calibrated and is in dB re: Pa/V units.)

attached to the duct. Secondly, the long throat of the JBL-2485 sources (approximately 0.12 m) means that there are a number of throat–duct resonances in the frequency range of interest. As discussed earlier, large reflections from the sources will occur at the anti-resonances of the throat and this means that at the anti-resonance frequencies the source farthest upstream (for example source 6) is very inefficient at driving sound downstream to the microphone. However, the source closest to the microphone (source 1) benefits from sound reflected off of the upstream sources and hence has improved efficiency. In general the sources farthest from the microphone are more ineffective since they have more passive 'obstacles' to overcome. Unless throat lengths are substantially reduced, or removed altogether, the addition of more sources will have little effect on the maximum achievable sound levels.

3.3. Single frequency excitation

Using the six measured transfer functions the optimal phasing required at any frequency in the range of interest could be calculated using Eq. (14). A series of tests were conducted at four discrete frequencies and the sound pressures monitored at the two downstream microphones (Duct #2 Fig. 1(b)). The sources were driven with independent, phase compensated, $30V_{RMS}$ signals. Although a single frequency was injected into the duct the very high levels achieved cause the sine waves to distort as they propagated. Fig. 11 shows the sound measured at both microphones when the sources were optimally phased and driven with a 1000 Hz signal. At this frequency the second microphone is nearly 20 wavelengths downstream and this is sufficiently far to allow shock waves ('N' waves) to develop [9]. The pressure level of the wave has also reduced significantly due to non-linear dissipation. This result shows that if high level sound is created in a duct it will only maintain its original shape and amplitude over a relatively short distance.

Table 1 shows the time averages sound level at both microphones (in dB re: 20 μPa RMS) at the fundamental drive frequency and then when all of the harmonics up to 6 kHz are included (6 kHz is the frequency set on the low pass filters before the data was acquired at 20 kHz). No information is included about the harmonic content of the 4 kHz test since none of the harmonics fall below 6 kHz. Levels in the order of 156 dB were achieved at 1, 2 and 3 kHz at microphone #1 but the levels at microphone #2 were substantially attenuated. The results presented show that

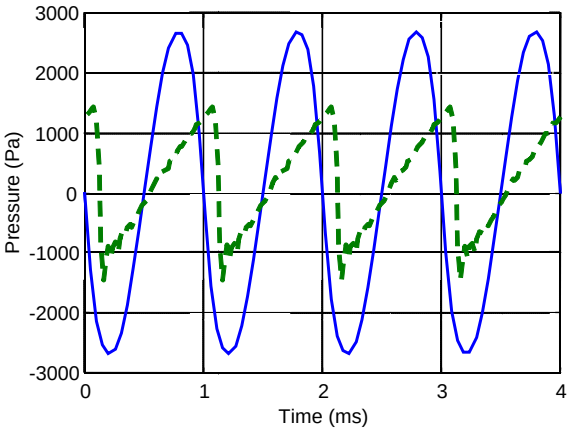

Fig. 11. The pressure measured at the two microphones in the duct when all six sources are optimally phased and driven at 1000 Hz mic 1 (—), mic 2 (- -). The non-linear propagation of the sound causes an "N" wave to develop by the time it reaches the second microphone.

Table 1
Sound pressure levels in dB rms re 20 μPa at microphones #1 near the source section and #2 further downstream

	Mic #1 (dB)		Mic#2 (dB)		Attenuation (dB)	
	Fundamental harmonic	Harmonics up to 6 kHz	Fundamental harmonic	Harmonics up to 6 kHz	Fundamental harmonic	Harmonics up to 6 kHz
1000 Hz	156.7	156.8	150.9	152.4	5.8	4.4
2000 Hz	156.1	156.5	145.8	147.4	10.7	9.1
3000 Hz	155.9	156.4	143.2	144.4	13.2	12.0
4000 Hz	147.5	—	150.0	—	−2.5	—

Higher frequencies show higher attenuation along the duct until cut-on.

below the cut-on of the first mode at 3.4 kHz higher frequencies tend to distort and attenuate more rapidly with distance due to shorter wavelengths. However, above cut-on (i.e., the 4 kHz case) the sound measured at microphone #2 is actually 2.5 dB higher than at microphone #1. A full understanding of this behavior will require further investigation but it is probably due to the interaction of the two propagating modes. Microphone #1 was probably in a location where the two propagating modes were out of phase with each other causing a lower than expected pressure level. The mode that is just cut-on also has a small wavenumber component in the z direction and this may affect the rate at which the 'N' waves develop and also affect the non-linear dissipative mechanism.

3.4. *Pulse generation: effort weighting and maximizing output*

Once the transfer functions (shown in Fig. 10) between the sources and the microphones are known then a few simple computational steps can be undertaken to determine the likely effect of conditioning (Eq. (26)) and loop optimization.

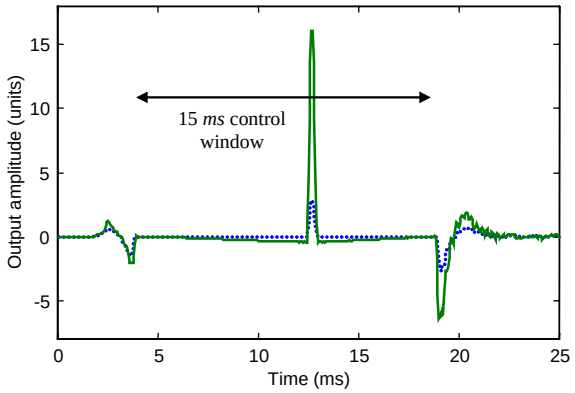

Fig. 12. The output predicted from measured data using six JBL sources with (—) and without conditioning (- -). By adding conditioning a six-fold increase in output was achieved with 1.5% error.

Consider, as an example, the case where the desired pulse is defined by a 0.5 ms long Hanning window. This pulse is imbedded in a 'control window' that is 15 ms long where it is desired that the pressure remain zero. With a 20 kHz sample rate this creates a 300 point desired output sequence inside which the 10 point pulse is imbedded. Using Eq. (26) the optimal input sequences $\mathbf{v_e}$ are calculated and can then be used to reconstruct the expected pulse using the measured impulse response functions. Fig. 12 shows two plots of the expected pulses when β is zero (i.e., zero error E) and when β is set such that the error E is 0.015 (or 1.5%). This example clearly shows that by adding a small conditioning term huge increases in performance can be achieved, a factor of 6 in this case, without significantly effecting the accuracy of the pulse. Inside the control window the pressure in both examples is well behaved and follows the desired pulse shape but outside of the 'control window', in the region that the algorithm does not consider, there can be large pressure pulses. The output window can be made as large as is necessary but this eventually runs into computational difficulties as it requires the inversion of a $J \times J$ matrix (Eq. (25) or (26)).

Fig. 13 shows the input voltages to the six sources used to create the pulse (with conditioning case) shown in Fig. 12. It should be noted that source #1 is driven with the largest peak voltage (normalized to unity) but all of the other sources have excess authority left. By removing source #1 from the calculation (i.e., $k = 2$–6) the input voltages to the remaining five sources that produce the same pulse can be calculated using Eq. (26). The new set of input voltages is scaled such that when added to the first set of voltages (all six) one of the five remaining inputs has a maximum of one. This source can then be removed from the calculation and the calculation repeated with four sources and so on until there are no remaining sources. This loop optimization leads to an increase (in this example) in pulse size of 45% without changing the accuracy with which the pulse is created. The pulses created with and without loop optimization are shown in Figs. 14 and 15 shows the new set of normalized input voltages that create the larger pulse all with a peak voltage (normalized) of one.

For the creation of pulses, peak voltage may not be the only criteria that limits the maximum performance of actuators. Other criteria such as maximum diaphragm displacement or energy input integrated over the pulse could be alternative (and possibly better) criteria but further work

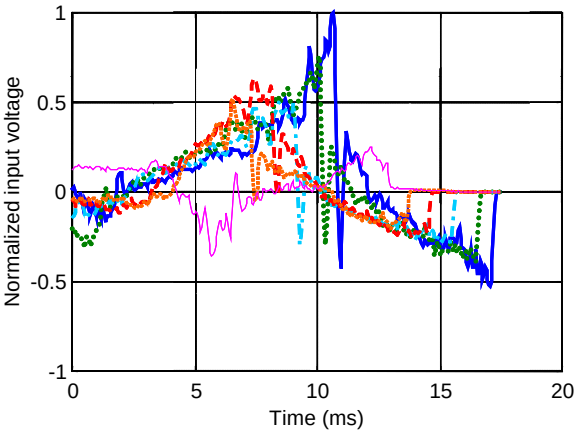

Fig. 13. The input voltages to the six sources used to create the pulse shown in Fig. 12 (with conditioning). Input ♯ 1 (—) is the only source to be maximized.

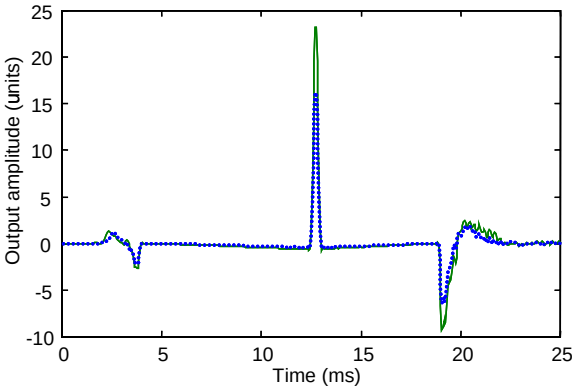

Fig. 14. The output predicted from measured data using six JBL sources with (—) and without (- -) loop optimization. By maximizing the input levels to all six sources (loop optimization) an additional 45% of output was achieved.

will be required to determine whether this is true or not. This loop optimization method can then be applied to any of these alternative criteria.

3.5. *Pulse generation: experimental results*

In the experiments conducted a 0.5 ms (i.e., ten points with a 20 kHz sample rate) Hanning window was used as the desired pulse shape. This pulse was imbedded in an 8 ms long control window and the conditioning coefficient β was chosen such that the error coefficient was kept below 10%. The pulse created using all six JBL sources was recorded at both microphones and is shown in Fig. 16. The pulse measured as it passes the first microphone has a maximum pressure of 6500 Pa which is 170 dB relative to 20 μPa. The pulse at this point is already distorted and by the time it reaches the second microphone it is a fully developed shock wave. The amplitude of the pulse has by this point reduced to 4100 Pa which is 166 dB relative to 20 μPa. It is interesting to

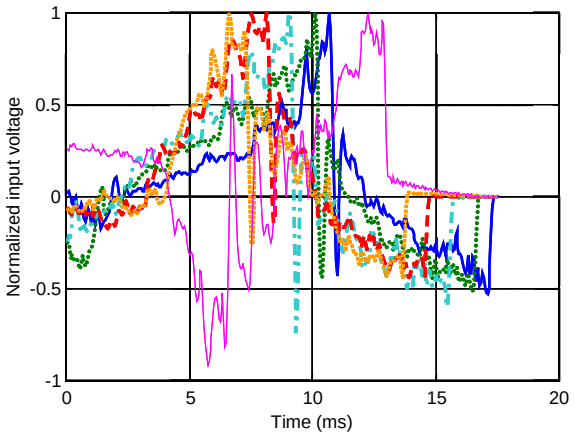

Fig. 15. The input voltages to the six sources used to create the 'loop optimized' pulse shown in Fig. 14. The output from all sources are now maximized.

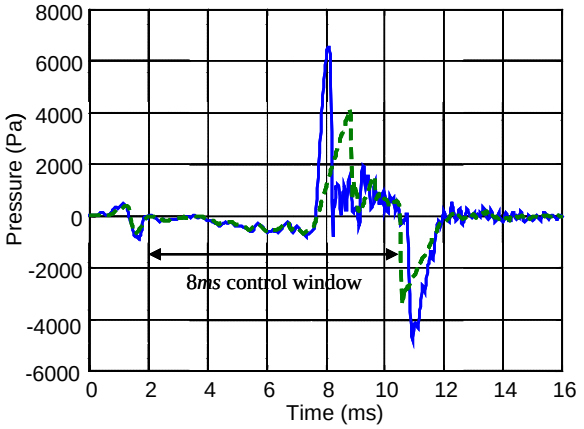

Fig. 16. The pulse measured at both microphones. Mic #1 (—), near the source section, measures a pulse with maximum amplitude over 6500 Pa and Mic #2 (- -) farther downstream measured a shock wave with a peak value around 4000 Pa.

note that there is also a negative shock wave which occurs outside the control window and because the negative shock wave travels more slowly than the positive shock wave the two shocks are closer together at mic#2 than at mic#1.

4. Conclusions

This paper first develops a simple model of a source driving into a duct through a short throat (Fig. 3) using an impedance approach. The acoustics in the duct itself are modelled using a series

of propagating and non-propagating acoustic modes. As is well known, near the cut-on of each acoustic mode the duct input impedance becomes very large. This has the effect of restricting the velocity at the throat–duct interface. Under these circumstances the source diaphragm compresses the air in the compliant throat. Just above cut-on the reduced velocity at the duct-throat interface can still create large pressures downstream because the newly cut-on mode has a large acoustic transfer impedance (Eq. (11)). However, just below this cut-on the new mode is still not propagating over significant distances and the pressure downstream is due to the propagation of the lower order modes (that are well above their cut-on). Therefore, the reduced duct-throat velocity results in a reduced pressure level downstream by restricting the amplitude of the modes that are already cut-on. This phenomenon is termed the pre cut-on loading effect and can only be overcome if the throat lengths are reduced. The pre cut-on loading effect was measured experimentally using both Selenium DH200-HM sources and JBL-2485 sources. The effect was more pronounced for the JBL sources that have significantly longer throat lengths. Large throats also act as passive reflectors and it was shown experimentally that the sources farthest upstream in an array were the most inefficient at generating waves downstream especially at anti-resonance frequencies (for example 1100 Hz). These results imply that better designed actuators with very short throat lengths could remove some of the undesirable dynamics from the frequency range of interest.

Above cut-on the interaction of the propagating modes create peaks and troughs in the frequency response of the microphone (Figs. 6 and 9). This is because the modes travel with different phase speed down the duct and their interaction can be both re-enforcing (peaks) or cancelling (troughs) at any one position. Multiple sources tend to alleviate this problem because each source will excite the first cut-on mode with a different relative phase to the plane wave mode.

Given a specific source configuration the objective was to maximize the sound in the duct without exceeding the power constraints of the sources. In this paper the pressure downstream in the duct is considered as a set of voltage signals (used to drive the sources) that are filtered by a set of measurable transfer functions. The transfer functions between six JBL-2485 compression drivers attached to a duct and a downstream microphone were measured and used to calculate the optimal input voltages.

A frequency domain method was developed to maximize the sound in the duct when driven with a harmonic excitation. At a given frequency all of the sources are driven with the same amplitude (maximum allowable amplitude) but with the negative phase of their respective transfer functions. This phase compensation results in all of the signals from all of the sources reaching the microphone in phase and the resulting amplitude is proportional to the sum of the amplitudes of all of the transfer functions at that frequency (Eq. (15)). Using a National Instruments eight channel output card (*PCI-6713*), six independent drive signals were amplified and used to drive the six sources with a single frequency, phase compensated, $30 V_{RMS}$ signal. The sound pressure levels measured at the downstream microphone were over 155 dB for signals between 1000 and 4000 Hz. At these levels the pressure is large enough to create 'N' waves over relatively short distances and these were measured at microphone #2 6.5 m downstream (Fig. 11).

To create a pressure pulse in the duct a time domain inverse method was used. By considering both the input (voltages) and output (pressure) signals to be of finite duration the problem could be formulated using a time domain matrix method. By choosing the appropriate input signals any

desired output could be achieved. For this work a 0.5 ms Hanning pulse, imbedded in a larger control window, was chosen as the desired output. Using this formulation the problem was underdetermined, that is, there was no unique solution and there is a large set of inputs that create the same output. In view of the voltage limitations of the sources it was decided that a good solution would be the one that used the minimum amount of input voltage (defined as the averaged voltage squared level). There is in this case a unique solution. Even using this voltage minimizing technique large input voltages are required for modest output levels and this is due to poor conditioning of the $\mathbf{HH}^{\mathbf{T}}$ matrix. To overcome this a conditioning factor was added ($\mathbf{HH}^{\mathbf{T}}+\boldsymbol{\beta}\mathbf{I}$) that greatly improved the efficiency of the sources at the expense of accuracy. However, it was shown (using measured data) that a small amount of conditioning, which lead to only a 1.5% error in reproduction, created a six-fold increase in output level. There is a clear trade-off between accuracy of reproduction and sound level achieved. In an attempt to further optimize the output a loop optimization routine was developed that used up the excess authority in the sources. After loop optimization all of the sources have the same peak voltage and using this routine a 45% increase in output was achieved over a non-optimized case. Using this method the output card was again used to create six drive signals. A 0.5 ms pressure pulse with a maximum pressure level over 6500 Pa was achieved experimentally in the duct. This sound pressure level was sufficiently high to create shock waves.

This paper demonstrated that using off the shelf compression drivers, arranged in an axial array, very high level sound could be created in a small duct in anechoic (or semi-anechoic) conditions. The pressure levels achieved were large enough to create large non-linear effects. Improvements to the design of the drivers (i.e., shorter throats) will increase the efficiency of the system and also lead to flatter frequency response behavior.

Acknowledgements

The authors acknowledge the Structural Acoustics Branch, NASA Langley Research Center, for supporting this work and especially thank Mike Jones, Tony Parrott and Brian Howerton for their help in conducting the experiments presented in this paper. We also thank Rick Wright for creating software associated with running the tests.

References

[1] S.J. Elliott, P.A. Nelson, Multiple point equalization in a room using adaptive digital filters, *Journal of Audio Engineering Society* 37 (1) (1989) 899–907.
[2] D.E. Brown, B.M. Sullivan, Adaptive equalization of the acoustic response in the NASA Langley sonic boom chamber, *Proceedings of Recent Advances in Active Control of Sound, Vibration*, 1991, pp. 360–371.
[3] R.E.D. Bishop, D.C. Johnson, *The Mechanisms of Vibration*, Cambridge University Press, Cambridge, 1960.
[4] F. Tse, I. Morse, R. Hinkle, *Mechanical Vibration Theory and Application*, Prentice-Hall, Englewood Cliffs, NJ, 1978.
[5] L.E. Kinsler, A.R. Frey, A.B. Coppens, J.V. Sanders, *Fundamentals of Acoustics*, Wiley, NewYork, 1950.
[6] F. Fahy, *Foundations of Engineering Acoustics*, Academic Press, NewYork, 2001.
[7] L. Meirovitch, *Elements of Vibration Analysis*, McGraw-Hill, New York, 1986.

[8] J.P. Smith, R.A. Burdisso, The Application of the Herschel–Quinke Tube Concept for the Reduction of Tonal and Broadband Noise from Turbofan Engines, NASA, 1999 (VPI-ENGR.98.167, contract #98-0448-10)
[9] P.M. Morse, K.U. Ingard, *Theoretical Acoustics*, McGraw-Hill, New York, 1986.
[10] P.A. Nelson, S.J. Elliott, *Active Control of Sound*, Academic Press, New York, 1993.
[11] S.J. Elliott, I.M. Stothers, P.A. Nelson, Amultiple error LMS algorithm and its application to the active control of sound and vibration, *IEEE Transactions on Acoustics, Speech, and Signal Processing* 35 (1987) 1423–1434.
[12] M. Tohyama, T. Koike, *Foundations of Acoustic Signal Processing*, Academic Press, New York, 1998.
[13] O. Kirkeby, P.A. Nelson, F. Orduna-Bustamente, H. Hamada, Local sound field reproduction using digital signal processing, *Journal of the Acoustical Society of America* 100 (3) (1996) 1584–1593.
[14] P.A. Nelson, O. Kirkeby, T. Takeuchi, H. Hamada, Sound fields for the production of virtual acoustic images, *Journal of Sound and Vibration* 204 (2) (1997) 386–396.
[15] A.V. Oppenheim, R.W. Schafer, *Digital Signal Processing*, Prentice-Hall, Englewood Cliffs, NJ, 1975.
[16] M.E. Johnson, S.J. Elliott, K-H Baek, J.Garcia-Bonito, An equivalent source technique for calculating the sound field inside an enclosure containing scattering objects, *Journal of the Acoustical Society of America* Part 1 104 (3) (1998) 1221–1231.